Journal of Statistical Mechanics: Theory and Experiment
An IOP and SISSA journal

Finite temperature behavior of strongly disordered quantum magnets coupled to a dissipative bath*

G Schehr[1] **and H Rieger**[2]

[1] Laboratoire de Physique Théorique, Université de Paris-Sud, F-91405 Orsay, France
[2] Theoretische Physik, Universität des Saarlandes, D-66041 Saarbrücken, Germany
E-mail: Gregory.Schehr@th.u-psud.fr and h.rieger@mx.uni-saarland.de

Received 19 November 2007
Accepted 14 March 2008
Published 11 April 2008

Online at stacks.iop.org/JSTAT/2008/P04012
doi:10.1088/1742-5468/2008/04/P04012

Abstract. We study the effect of dissipation on the infinite randomness fixed point and the Griffiths–McCoy singularities of random transverse Ising systems in chains, ladders and in two dimensions. A strong disorder renormalization group scheme is presented that allows the computation of the finite temperature behavior of the magnetic susceptibility and the spin specific heat. In the case of ohmic dissipation the susceptibility displays a crossover from Griffiths–McCoy behavior (with a continuously varying dynamical exponent) to classical Curie behavior at some temperature T^*. The specific heat displays Griffiths–McCoy singularities over the whole temperature range. For super-ohmic dissipation we find an infinite randomness fixed point within the same universality class as the transverse Ising system without dissipation. In this case the phase diagram and the parameter dependence of the dynamical exponent in the Griffiths–McCoy phase can be determined analytically.

Keywords: dissipative systems (theory), quantum phase transitions (theory), disordered systems (theory)

* Dedicated to Professor Thomas Nattermann on the occasion of his 60th anniversary.

©2008 IOP Publishing Ltd and SISSA
1742-5468/08/P04012+23$30.00

Contents

1. Introduction

The interplay between quantum fluctuations and quenched disorder in the form of an extensive amount of impurities or other random spatial inhomogeneities can lead to a new class of quantum phase transitions, governed by an infinite randomness fixed point (IRFP) as established for transverse Ising models [1] and many other disordered quantum systems (for an overview see [2]). Besides unusual scaling laws *at* the transition the IRFP is characterized by a whole parameter range *around* the transition, in which physical observables display singular and even divergent behavior in spite of a finite spatial correlation length. This is the manifestation of Griffiths–McCoy singularities or quantum Griffiths behavior [3]–[7]. They have their origin in rare regions of strongly coupled spins (or other quantum mechanical degrees of freedoms) that tend to order locally and thus produce a strong response to small external fields, long relaxation (or tunneling) times and small excitation energies.

If the underlying quantum phase transition is governed by an infinite randomness fixed point the statistics of these rare events leads to a power law divergence of the susceptibility in a region around the quantum critical point with a continuously varying exponent. This dynamical exponent determines all singularities in the Griffiths–McCoy phase. Continuously varying exponents, interrelated in a specific way for different physical observables, were observed in many heavy-fermion materials and it was argued that this is a manifestation of Griffiths–McCoy behavior due to an underlying IRFP [8, 9]. In essence

J. Stat. Mech. (2008) P04012

these systems form local moments that interact via long-range RKKY interaction and have a strong Ising anisotropy, such that an effective model describing these degrees of freedom and their interaction is a random transverse Ising system.

Later it was argued that, due to the interaction via band electrons, the effective spin degrees of freedom are strongly coupled to a dissipative ohmic bath [10, 11]. From this point of view the rare regions should be described by spin-boson systems, which are known to behave classically for sufficiently strong coupling to the dissipative bath [12], which would destroy the expected Griffiths–McCoy singularities.

Since in the presence of dissipation rare regions can undergo phase transitions and freeze independently from one another (like in the McCoy–Wu model in the mean field approximation [13]), the global phase transition of the system is destroyed by smearing because different spatial parts of the system order at different values of the control parameter [14, 15].

Recently we analyzed the random transverse Ising chain coupled to a ohmic dissipative bath with a strong disorder renormalization group (SDRG) scheme and could demonstrate that the transition is indeed smeared, but argued that Griffiths–McCoy singularities are still observable, at least down to very low temperatures also in the presence of dissipation [16]. This was done by analyzing the gap and cluster distribution. In this paper we continue and extend this SDRG study by (a) analyzing the low temperature behavior of the magnetic susceptibility and the spin specific heat in the case of ohmic dissipation, where we will argue that Griffiths–McCoy singularities are visible at all temperatures in the specific heat and above a (small) crossover temperature in the susceptibility; (b) considering in addition to chains also ladders and two-dimensional systems, where we obtain similar results as for the chain; and (c) applying the SDRG also to super-ohmic dissipation, where we find a quantum phase transition belonging to the same IRFP universality class as the system without dissipation and compute analytically the phase diagram and dynamical exponent in the Griffiths–McCoy phase.

The system that we study is the random transverse Ising model where each spin is coupled to a dissipative bath of harmonic oscillators, i.e. ferromagnetically coupled spin-boson systems [12]. It is defined on a d-dimensional square lattice of linear size L with periodic boundary conditions (pbc) and described by the Hamiltonian

$$H = -\sum_{\langle i,j\rangle} J_{ij}\sigma_i^z\sigma_j^z - \sum_i \left[h_i\sigma_i^x + \sum_k \left(C_{k,i}\hat{x}_{k,i}\sigma_i^z + \frac{\hat{p}_{k,i}^2}{2} + \omega_{k,i}^2\frac{\hat{x}_{k,i}^2}{2}\right)\right], \quad (1)$$

where $\sigma_i^{x,z}$ are Pauli matrices and the masses of the oscillators are set to one. The quenched random bonds J_i (respectively random transverse field h_i) are uniformly distributed between 0 and J_0 (respectively between 0 and h_0). The properties of the bath are specified by its spectral function $\mathcal{J}_i(\omega)$:

$$\mathcal{J}_i(\omega) = \frac{\pi}{2}\sum_k \frac{C_{k,i}^2}{\omega_{k,i}}\delta(\omega-\omega_{k,i}) = \frac{\pi}{2}\alpha_i\Omega_i^{1-s}\omega^s\theta(\Omega_i-\omega), \quad (2)$$

where Ω_i is a cutoff frequency and $\theta(x)$ is the Heaviside function such that $\theta(x) = 1$ if $x > 0$ and $\theta(x) = 0$ if $x < 0$. The case $s = 1$ is known as ohmic dissipation although $s > 1$ (respectively $s < 1$) corresponds to a super-ohmic (respectively sub-ohmic) dissipation. Initially the spin–bath couplings and cutoff frequencies are site-independent, i.e. $\alpha_i = \alpha$ and $\Omega_i = \Omega$, but both become site-dependent under renormalization.

J. Stat. Mech. (2008) P04012

2. Real space renormalization

2.1. Decimation procedure

In this section, we derive in detail the real space renormalization scheme to study the dissipative random transverse Ising model as in equation (1). For simplicity, we present the calculation in dimension $d = 1$ (extensions to higher dimensions are discussed below) and focus on the random transverse Ising chain (RTFIC):

$$H_{1d} = \sum_{i=1}^{L} \left[-J_i \sigma_i^z \sigma_{i+1}^z - h_i \sigma_i^x + \sum_k \left(C_{k,i} \hat{x}_{k,i} \sigma_i^z + \frac{\hat{p}_{k,i}^2}{2} + \omega_{k,i}^2 \frac{\hat{x}_{k,i}^2}{2} \right) \right]. \tag{3}$$

To characterize the ground state properties of this system (1), we follow the idea of a real space renormalization group (RG) procedure introduced in [17] and pushed further in the context of the RTFIC without dissipation in [3]. The strategy is to find the largest coupling in the chain, either a transverse field or a bond, compute the ground state of the associated part of the Hamiltonian and treat the remaining couplings in perturbation theory. The bath degrees of freedom are dealt with in the spirit of the 'adiabatic renormalization' introduced in the context of the (single) spin-boson (SB) model [12], where it describes accurately its critical behavior [18].

2.1.1. When the largest coupling is a bond. Suppose that the largest coupling in the chain is a bond, say J_2. The associated part H_2 of the full Hamiltonian H_{1d} in equation (3) is

$$\begin{aligned} H_2 &= H_2^{(0)} + V, \\ H_2^{(0)} &= -J_2 \sigma_2^z \sigma_3^z + \sum_{i=2,3} \sum_k \left(C_{k,i} \hat{x}_{k,i} \sigma_i^z + \frac{\hat{p}_{k,i}^2}{2} + \omega_{k,i}^2 \frac{\hat{x}_{k,i}^2}{2} \right), \\ V &= -h_2 \sigma_2^x - h_3 \sigma_3^x. \end{aligned} \tag{4}$$

Let us first focus on $H_2^{(0)}$ in equation (4) and first introduce the notation for the spin part $|\mathbf{S}\rangle \equiv |S_2, S_3\rangle$, with $S_i = \pm 1$ such that $\sigma_i^z |\mathbf{S}\rangle = S_i |\mathbf{S}\rangle$ for $i = 2, 3$. Considering now the two baths on site $i = 2, 3$, respectively, they are composed of a set of harmonic oscillators which are labeled by an integer k (which formally runs from 0 to ∞) and by $i = 2, 3$. We denote by $|n_{k,i}\rangle$ the eigenvalues of these harmonic oscillators such that

$$\left(\frac{\hat{p}_{k,i}^2}{2} + \omega_{k,i}^2 \frac{\hat{x}_{k,i}^2}{2} \right) |n_{k,i}\rangle = \left(n_{k,i} + \frac{1}{2} \right) \omega_{k,i} |n_{k,i}\rangle. \tag{5}$$

In the absence of the coupling between the spins and the bath, $H_2^{(0)}$ can be straightforwardly diagonalized by tensorial products of $|\mathbf{S}\rangle$ and $|n_{k,i}\rangle$. The corresponding eigenvalues are simply the sum of the eigenvalues of the individual Hamiltonians in equation (4) without the last term of the interaction. The coupling between the spins and the baths does not change these eigenvalues (up to a global shift) and only affects the eigenstates. We introduce the shifted 'eigenvectors'

$$|n_{k,j}^{\pm}\rangle = \exp\left(\pm i \frac{C_{k,j}}{\omega_{k,j}^2} \hat{p}_{k,j} \right) |n_{k,j}\rangle, \qquad j = 2, 3, \tag{6}$$

J. Stat. Mech. (2008) P04012

from which we can construct the eigenvectors of $H_2^{(0)}$, including the interaction between the baths and the spins as

$$|\mathbf{S},\mathbf{n}\rangle = |S_2,S_3\rangle \otimes |\mathfrak{n}_2^{S_2}\rangle \otimes |\mathfrak{n}_3^{S_3}\rangle,$$
$$|\mathfrak{n}_i^{S_i}\rangle = \bigotimes_k |n_{k,i}^{S_i}\rangle. \tag{7}$$

The eigenvalues of $H_2^{(0)}$ are given by

$$H_2^{(0)}|\mathbf{S},\mathbf{n}\rangle = E_{\mathbf{S},\mathbf{n}}^{(0)}|\mathbf{S},\mathbf{n}\rangle,$$
$$E_{\mathbf{S},\mathbf{n}}^{(0)} = -J_2 S_2 S_3 + \sum_{i=2,3}\sum_k \left[\left(n_{k,i}+\frac{1}{2}\right)\omega_{k,i} - \frac{1}{2}\frac{C_{k,i}^2}{\omega_{k,i}^2}\right]. \tag{8}$$

Each level is thus *a priori* degenerated twice (except accidental degeneracy) and in the limit of large coupling J_2 we first restrict ourselves to the lowest energy levels, such that $S_2 S_3 = +1$. Performing perturbation theory in V, one obtains that the first-order corrections vanish. To second order in V, one has to diagonalize the 2×2 matrix $V^{(2)}$ in the eigensubspace associated with the zeroth-order eigenvalue $E_{\mathbf{S},\mathbf{n}}^{(0)}$ with $S_2 S_3 = +1$ which is formally given by

$$V^{(2)} = \sum_{\mathbf{S}',\mathbf{n}',E_{\mathbf{S}',\mathbf{n}'}\neq E_{\mathbf{S},\mathbf{n}}} \frac{V|\mathbf{S}',\mathbf{n}'\rangle\langle\mathbf{S}',\mathbf{n}'|V}{E_{\mathbf{S},\mathbf{n}}^{(0)} - E_{\mathbf{S}',\mathbf{n}'}^{(0)}}. \tag{9}$$

One obtains from (9) the diagonal elements

$$V_{11}^{(2)} = V_{22}^{(2)} = h_2^2 \sum_{\mathfrak{n}_2'} \frac{|\langle \mathfrak{n}_2^+|\mathfrak{n}_2'^-\rangle|^2}{-2J_2 + \sum_k (n_{k,2}-n_{k,2}')\omega_{k,2}} + h_3^2 \sum_{\mathfrak{n}_3'} \frac{|\langle \mathfrak{n}_3^+|\mathfrak{n}_3'^-\rangle|^2}{-2J_2 + \sum_k (n_{k,3}-n_{k,3}')\omega_{k,3}}, \tag{10}$$

and the off-diagonal elements

$$V_{12}^{(2)} = V_{21}^{(2)} = -\frac{h_2 h_3}{J_2}\langle \mathfrak{n}_2^-|\mathfrak{n}_2^+\rangle\langle \mathfrak{n}_3^-|\mathfrak{n}_3^+\rangle. \tag{11}$$

In the absence of a coupling to the dissipative bath (i.e. $C_{k,i}=0$ for all k and i) the shifted eigenstates (6) are identical with the non-shifted eigenstates and therefore $\langle \mathfrak{n}_i^-|\mathfrak{n}_j^+\rangle = \delta_{\mathfrak{n}_i,\mathfrak{n}_j}$ and thus $V_{11}^{(2)} = V_{22}^{(2)} = (h_1^2 + h_2^2/-2J_2)$ and $V_{12}^{(2)} = V_{21}^{(2)} = -h_2 h_3/J_2$. This matrix has two eigenvalues whose difference, the gap, is $2h_2h_3/J_2$. Thus for each oscillator state the low lying excitations of H_2 in (4), with $S_2 = S_3$, can again be described by an effective two-state system, i.e. a spin in a transverse field of strength $h' = h_2 h_3/J_2$. The spirit of the strong disorder renormalization group is to keep this effective two-level system (for each oscillator state) and to neglect the large energy doublet with $S_2 \neq S_3$. In this way one has replaced two spins (with moments μ_2 and μ_3) and a large coupling J_2 between them by a single effective spin with moment $\mu_2+\mu_3$ in a small transverse field h_2h_3/J_2; thus one degree of freedom with a large energy has been decimated.

In the presence of non-vanishing couplings $C_{k,i}$ to the oscillators one needs to decimate also the high energy modes of the bath such that $\omega_{k,i} > pJ_2$, where p is some (large)

J. Stat. Mech. (2008) P04012

number. Given that J_2 is a large energy scale, the low lying energy levels will be those with $n_{k,i} = 0$ for $\omega_{k,i} > pJ_2$. Therefore we decompose the oscillator states according to

$$|\mathfrak{n}_i^S\rangle = |\mathfrak{n}_i^{<S}\rangle \otimes |\mathfrak{n}_i^{>S}\rangle, \tag{12}$$

with $S = \pm 1$ and

$$|\mathfrak{n}_i^{<S}\rangle = \bigotimes_{k_i^<} |n_{k_i}^S\rangle \qquad \text{and} \qquad |\mathfrak{n}_i^{>S}\rangle = \bigotimes_{k_i^>} |n_{k_i}^S\rangle, \tag{13}$$

where $k_i^< = \{k|\omega_{k,i} \leq pJ_2\}$ and $k_i^> = \{k|\omega_{k,i} > pJ_2\}$. Additionally we introduce the product state of oscillators which are in the ground state by $|\mathfrak{o}_i^{>S_i}\rangle = \bigotimes_{k_i^>} |0_{k_i}^{S_i}\rangle$. At energy scales smaller than pJ_2 all oscillators with frequencies larger than pJ_2 will be in their ground states, and therefore we will consider the matrix elements in (10) and (11) only for oscillator states $|\mathfrak{n}^+\rangle = |\mathfrak{n}^{<+}\rangle \otimes |\mathfrak{o}^{>+}\rangle$. For these states the two sums on the rhs of (10) are

$$\sum_{\mathfrak{m}_i^<, \mathfrak{m}_i^>} h_i^2 \frac{|\langle \mathfrak{n}_i^{<+}|\mathfrak{m}_i^{<-}\rangle|^2 \cdot |\langle \mathfrak{o}_i^{>+}|\mathfrak{m}_i^{>-}\rangle|^2}{-2J_2 - \sum_{k^>} m_{k,2}\omega_{k,2} + \sum_{k^<}(n_{k,2} - m_{k,2})\omega_{k,2}}. \tag{14}$$

To leading order in J_2 one can neglect the term $\sum_{k^<}(n_{k,2} - m_{k,2})\omega_{k,2}$, since it involves only frequencies smaller than pJ_2. Then the sum over the low frequency oscillator states $|\mathfrak{m}_i^<\rangle$ yields one since they form a complete basis for the low frequency oscillator Hilbert space and the individual terms in the sum do not depend on the quantum numbers $\mathfrak{n}_i^<$ any more. Thus the diagonal matrix elements in (10) are, to leading order in J_2:

$$V_{ii}^{(2)} = h_2^2 \sum_{\mathfrak{m}_2^>} \frac{|\langle \mathfrak{o}_2^{>+}|\mathfrak{m}_2^{>-}\rangle|^2}{-2J_2 - \sum_{k_2^>} m_{k_2}\omega_{k,2}} + h_3^2 \sum_{\mathfrak{m}_3^>} \frac{|\langle \mathfrak{o}_3^{>+}|\mathfrak{m}_3^{>-}\rangle|^2}{-2J_2 - \sum_{k_3^>} m_{k_3}\omega_{k,3}}. \tag{15}$$

Note that this expression does not depend on the quantum numbers $\mathbf{n}^<$ for the low frequency oscillators. For the non-diagonal matrix elements in (11) one gets

$$V_{12}^{(2)} = V_{21}^{(2)} = -\frac{\mathcal{A}h_2h_3}{J_2}\langle \mathfrak{n}_2^{<-}|\mathfrak{n}_2^{<+}\rangle\langle \mathfrak{n}_3^{<-}|\mathfrak{n}_3^{<+}\rangle, \tag{16}$$

with

$$\mathcal{A} = \langle \mathfrak{o}_2^{>+}|\mathfrak{o}_2^{>-}\rangle\langle \mathfrak{o}_3^{>+}|\mathfrak{o}_3^{>-}\rangle = \prod_{k_2^>}\langle 0_{k_2}^+|0_{k_2}^-\rangle \prod_{k_3^>}\langle 0_{k_3}^+|0_{k_3}^-\rangle. \tag{17}$$

The amplitude $\mathcal{A}$ can then be expressed in terms of the spectral density, using that $\langle 0_{k,i}^+|0_{k,i}^-\rangle = \exp -(C_{k,i}^2/\omega_{k,i}^3)$. This yields

$$\mathcal{A} = \exp\left(-\frac{2}{\pi}\int_{pJ_2}^{\Omega_2}\frac{J_2(\nu)}{\nu^2}\,\mathrm{d}\nu - \frac{2}{\pi}\int_{pJ_2}^{\Omega_3}\frac{J_3(\nu)}{\nu^2}\,\mathrm{d}\nu\right), \tag{18}$$

where we have used the definition of the spectral density in equation (2). Since the diagonal term does not depend on $\mathbf{n}^<$ the diagonalization of $V^{(2)}$ yields (up to second order) the following correction to the lowest eigenvalues:

$$E_{\pm,\mathbf{n}^<}^{(2)} = \mathcal{E}_0 + \sum_{i=2,3}\sum_k \left(n_{k,i} + \frac{1}{2}\right)\omega_{k,i} \pm \frac{\mathcal{A}h_2h_3}{J_2}\langle \mathfrak{n}_2^{<-}|\mathfrak{n}_2^{<+}\rangle\langle \mathfrak{n}_3^{<-}|\mathfrak{n}_3^{<+}\rangle, \tag{19}$$

J. Stat. Mech. (2008) P04012

where $\mathcal{E}_0 = -J_2 + V_{11} - \frac{1}{2}\sum_{i=2,3}\sum_k C_{k,i}^2/\omega_{k,i}^2$ is a constant, independent of $\mathbf{n}^<$. We now consider an effective spin-boson Hamiltonian coupled to *both* baths 2 and 3:

$$\tilde{H}_2 = -\tilde{h}_2\sigma_2^x + \sum_{i=2,3}\sum_k\left(\frac{\hat{p}_{k,i}^2}{2} + \omega_{k,i}\frac{\hat{x}_{k,i}^2}{2} + C_{k,i}\hat{x}_{k,i}\sigma_2^z\right), \tag{20}$$

where the frequencies are such that $\omega_{k,i} < pJ_2$. The effective spins being coupled to both baths, one has

$$\tilde{\mathcal{J}}_2(\omega) = \theta(pJ_2 - \omega)(\mathcal{J}_2(\omega) + \mathcal{J}_3(\omega)). \tag{21}$$

Treating the small parameter $\tilde{h}_2$ in (degenerate) perturbation theory, one obtains the low lying eigenvalues of $\tilde{H}_2$ to first order in $\tilde{h}_2$:

$$\tilde{E}_{\pm,\mathbf{n}^<}^{(1)} = \sum_{i=2,3}\sum_k(n_{k,i} + \tfrac{1}{2})\omega_{k,i} \pm \tilde{h}_2\langle\mathfrak{n}_2^{<-}|\mathfrak{n}_2^{<+}\rangle\langle\mathfrak{n}_3^{<-}|\mathfrak{n}_3^{<+}\rangle. \tag{22}$$

The comparison between equations (19) and (22) shows that the low energy spectrum of the two interacting spin-bosons in H_2 can be described by a single spin-boson system with renormalized parameters given by

$$\tilde{h}_2 = \frac{\mathcal{A}h_2h_3}{J_2}, \tag{23}$$

$$\tilde{\alpha}_2 = \alpha_2 + \alpha_3, \qquad \tilde{\Omega}_2 = pJ_2, \tag{24}$$

where $\mathcal{A}$, which depends on the parameters of the Hamiltonian H_2, is given by equation (18) and the equalities in (24) are a direct consequence of equation (21). This effective spin-boson will interact ferromagnetically with the spin-boson on site 1 and site 4 with couplings

$$\tilde{J}_1 = J_1, \qquad \tilde{J}_2 = J_3. \tag{25}$$

These relations (23)–(25) constitute the first set of decimation rules.

2.1.2. When the largest coupling is a field. Suppose now that the largest coupling in the chain is a transverse field, say h_2. Before we treat the coupling of site 2 to the rest of the system $-J_1\sigma_1^z\sigma_2^z - J_2\sigma_2^z\sigma_3^z$ perturbatively as in [3] we consider the part of the Hamiltonian that represents a single spin-boson system:

$$H_2' = -h_2\sigma_2^x + \sum_k\left(\frac{\hat{p}_{k,2}^2}{2} + \omega_{k,2}\frac{\hat{x}_{k,2}^2}{2} + C_{k,2}\hat{x}_{k,2}\sigma_2^z\right). \tag{26}$$

In this case, one would like to have a way to decimate the high energy modes of the bath, here the harmonic oscillators, such that $\omega_{k,2} > ph_2$, where p is some (large) number. Since for those oscillators $\omega_{k,2} \gg h_2$ one can assume that they adjust instantaneously to the current value of σ_2^z, the renormalized energy splitting is easily calculated using equation (22)—the so-called adiabatic renormalization [12]—and one gets an effective

J. Stat. Mech. (2008) P04012

transverse field $\tilde{h}_2 < h_2$:

$$\tilde{h}_2 = \mathcal{A}' h_2, \qquad \tilde{\Omega}_2 = p h_2, \tag{27}$$

$$\mathcal{A}' = \exp\left(-\frac{2}{\pi}\int_{ph_2}^{\Omega_2} \frac{\mathcal{J}_2(\nu)}{\nu^2}\,\mathrm{d}\nu\right). \tag{28}$$

If $\tilde{h}_2$ is still the largest coupling in the chain the iteration (27) is repeated. Two situations may occur depending on the parameters s and α_i.

- If $s > 1$ or $s = 1$ and $\alpha_2 < 1$ this procedure (27) will converge to a finite value h_2^* given by

$$h_2^* = h_2 \exp\left(-\frac{2}{\pi}\int_{ph_2^*}^{\Omega_2} \frac{\mathcal{J}_2(\nu)}{\nu^2}\,\mathrm{d}\nu\right) \sim \begin{cases} h_2 \exp\left(-\dfrac{\alpha_2}{s-1}\right), & s > 1, \\ h_2 \left(\dfrac{p h_2}{\Omega_2}\right)^{\alpha_2/1-\alpha_2}, & s = 1, \quad \alpha_2 < 1, \end{cases} \tag{29}$$

  where the expression of h_2^* for $s > 1$ is valid only in the limit $ph_2 \ll \Omega_2$. In this case, the spin-boson system at site 2 is in a delocalized phase in which the spin and the bath can be considered as being decoupled (formally $\alpha_2 = 0$), as demonstrated by an RG treatment in [18]. If this value h_2^* (29) is still the largest coupling in the chain the spin on site 2 will be aligned with the transverse field. As in the RTFIC without dissipation, this spin is then decimated (as it will not contribute to the magnetic susceptibility) and gives rise, in second-order degenerate perturbation theory, to an effective coupling $\tilde{J}_1$ between the neighboring moments at sites 1 and 3 [3]:

$$\tilde{J}_1 = \frac{J_1 J_2}{h_2^*}. \tag{30}$$

- If $s = 1$ and $\alpha_2 > 1$, $\tilde{h}_2$ can be made arbitrarily small by repeating the procedure (27), implying that the SB system on site 2 is in its localized phase [18] and essentially behaves classically: the decimation rule (27) indeed amounts to setting $\tilde{h}_2 = 0$. Such a moment, or cluster of spins, will be aligned with an infinitesimal external longitudinal field and is denoted as 'frozen'.

These relations (27)–(30) constitute the second set of decimation rules. The complete decimation procedure is sketched for the ohmic case in figure 1.

2.2. Numerical implementation

In the following we analyze this RG procedure defined by the decimation rules (23)–(25) and (27)–(30) numerically. This is done by considering a finite system of linear size L with pbc and iterating the decimation rules until only one site is left. This numerical implementation has been widely used in previous works [2, 19] and it has been shown to reproduce with good accuracy the exact results of [3] for the RTFIC [19]. In particular, the transverse field h acting on the last remaining spin is, at low ferromagnetic coupling J_0, an estimate for the smallest excitation energy. Its distribution, $P_L(h/\Gamma_0)$, where Γ_0 is the largest coupling in the initial system of linear size L, reflects the characteristics of the

J. Stat. Mech. (2008) P04012

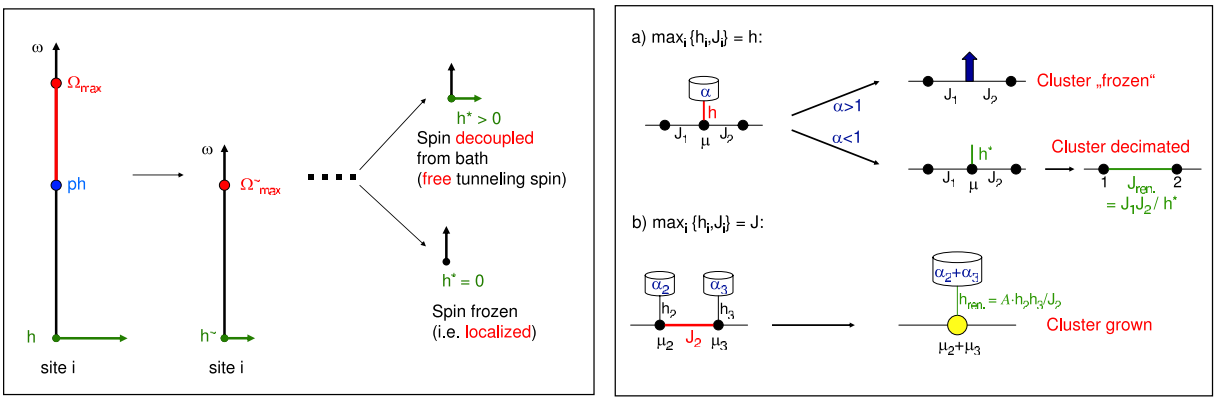

Figure 1. Left: sketch of the adiabatic renormalization of the bosonic bath for a single spin-boson system in the ohmic case: the fast oscillators with frequencies $\omega > ph$, where h is the transverse field acting on the spin and p is an arbitrary large parameter, are treated in the adiabatic approximation resulting in a renormalized transverse field $\tilde{h}$ for the spin and a decreased upper cutoff frequency $\tilde{\Omega}_{\max}$ for the bosonic bath. This procedure is continued until it runs into a fixed point, where either the renormalized field h^* vanishes (for $\alpha > 1$) and the spin is frozen, or the renormalized field h^* has a positive value, in which case it is a non-frozen spin in a transverse field h^*, decoupled from the bath. Right: sketch of the SDRG in the presence of a dissipative bath for the ohmic case. When a field h is the largest coupling (top), first the oscillator bath is renormalized along the lines sketched on the left site. Once this is done and the field is still the largest coupling the spin gets decimated as described in the text. When a bond J between two spins at sites 2 and 3 is the largest coupling the two spins get decimated to form a cluster with moment $\mu_2 + \mu_3$, coupled to a combination of baths 2 and 3, i.e. a new dissipative bath with coupling strength $\alpha_2 + \alpha_3$.

gap distribution [5]. This quantity, and specifically its dependence on the system size L, can be efficiently used to characterize Griffith–McCoy singularities and critical behavior characterized by an infinite randomness fixed point.

3. Ohmic dissipation

Ohmic dissipation means $s = 1$ in (2), i.e. a spectral function for the oscillators that is linear in the frequency (up to the upper cutoff Ω). For a single spin in a transverse field h and coupled to such an ohmic bath, a lot of results are available [12]. Here we mention only that this system has a phase transition at zero temperature driven by the coupling strength α. For small α the spin can still tunnel quantum mechanically, whereas for large α the spin is frozen and behaves classically, the critical coupling strength $\alpha_c(h)$ is equal to 1 in the limit where $h/\Omega \ll 1$ where Ω is the cutoff frequency of the bath, an exact result predicted correctly by the adiabatic approximation mentioned above. Such a transition is also present in an infinite ferromagnetic spin chain coupled to a dissipative bath, as was shown recently numerically [20]. Here we want to focus on the interplay of disorder, quantum fluctuations and dissipation and study random transverse field Ising

J. Stat. Mech. (2008) P04012

systems coupled to a dissipative environment by implementing the decimation rules (23)–(25) and (27)–(30) for ohmic dissipation. For $s = 1$, the amplitudes $\mathcal{A}$ in equation (18) and $\mathcal{A}'$ in equation (28) which enter these decimation rules are given by

$$\mathcal{A} = \left(\frac{pJ_2}{\Omega_2}\right)^{\alpha_2}\left(\frac{pJ_2}{\Omega_3}\right)^{\alpha_3}, \qquad \mathcal{A}' = \left(\frac{ph_2}{\Omega_2}\right)^{\alpha_2}. \tag{31}$$

3.1. One-dimensional system: random transverse field Ising chain

3.1.1. Gap distribution: finite size analysis. The RTFIC coupled to a ohmic bath was treated in detail in [16]. We just recall here the main results. Since the last spin can either be frozen (i.e. the last field h is zero) or non-frozen we split $P_L(h/\Gamma_0)$ into two parts:

$$P_L(h/\Gamma_0) = A_L\tilde{P}_L(h/\Gamma_0) + (1 - A_L)\delta(h/\Gamma_0), \tag{32}$$

where $\tilde{P}_L(h/\Gamma_0)$ is the restricted distribution of the last fields in the samples that are non-frozen and A_L is the fraction of these samples. It, or equivalently $\tilde{P}_L(\log(\Gamma_0/h))$, represents the distribution of the smallest excitation energy in the ensemble of non-localized spins. At low coupling (small J_0 or small α), $\tilde{P}_L(\log(\Gamma_0/h))$ shows indications of Griffiths–McCoy singularities characterized by the following scaling behavior for $\tilde{P}_L$:

$$\tilde{P}_L(\log(\Gamma_0/h)) = \mathcal{P}(\log(\Gamma_0/hL^z)), \tag{33}$$

where z is a dynamical exponent continuously varying with (J_0, α, etc). As the coupling is increased, z is also increasing and eventually, at some pseudo-critical point, $\tilde{P}_L(\log(\Gamma_0/h))$ exhibits a scaling which is characteristic for an IRFP:

$$\tilde{P}_L(\log(\Gamma_0/h)) = L^{-\psi}\mathcal{P}_{\mathrm{IRFP}}(L^{-\psi}\log(\Gamma_0/h)), \tag{34}$$

with $\psi \simeq 0.32$ [16] as a critical exponent characterizing the IRFP. Notice that this value of ψ is different from $\psi_{\mathrm{RTFIC}} = 1/2$ computed exactly for the RTFIC [3]. The main striking point in the case of ohmic dissipation is that, although the restricted distribution $\tilde{P}_L(\log(\Gamma_0/h))$ displays Griffith's like behavior as in equation (33), the magnetization becomes *finite* above a certain length scale L^*. This finite magnetization is a manifestation of the 'frozen' clusters which lead to the concept of rounded quantum phase transitions in the presence of dissipation [14]. Due to these 'frozen' clusters, the amplitude A_L decays exponentially above L^*, with $A_L \propto \mathrm{e}^{-L/L^*}$. However, as we pointed out in [16], the interpretation of the finite size analysis (32)–(34) in the presence of dissipation has to be done carefully. Indeed, in [16] we suggested that, despite the presence of these frozen clusters, Griffith's singularities should be observable in the susceptibility $\chi(T)$, above a certain temperature $T^* \propto L^{*-z}$, as well as in the specific heat $C_v(T)$. This property can actually be shown (see the appendix) on a toy model where one considers an RTFIC without dissipation but with a finite fraction ρ of zero transverse fields.

Here we will use this strong disorder approach to extract thermodynamical properties of the full problem described by the Hamiltonian (3).

J. Stat. Mech. (2008) P04012

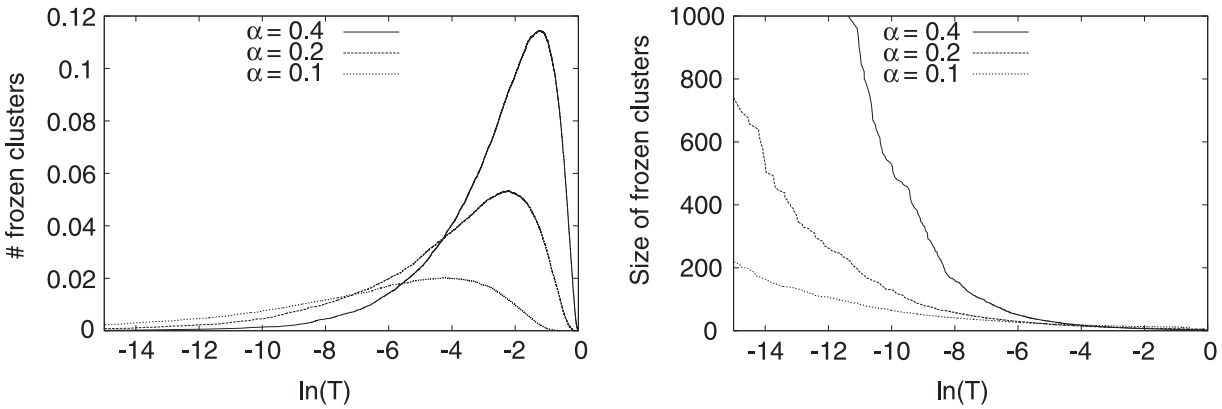

Figure 2. Number (left) and size (right) of frozen clusters in the disordered chain coupled to an ohmic bath as a function of temperature T for different values of α. Shown are data for a single large disorder realization, the size is $L = 40\,000$, the disorder strength is $h_0 = 1$ and $J_0 = 0.025$. For this value of J_0 the pseudo-critical point is located at $\alpha = 0.2$ [16].

3.1.2. Susceptibility at finite temperatures. The SDRG successively eliminates degrees of freedom with a large excitation energy from the starting Hamiltonian, thereby reducing continuously the maximum energy scale of the effective Hamiltonian. If continued down to the smallest energy scale the final effective Hamiltonian (consisting only of a single but large cluster in an effective transverse field) provides information about the ground state of the starting spin chain, the gap, the size, the geometry, etc, of the smallest excitation energy. To extract information on thermodynamic properties, at low but non-vanishing temperatures, one has to stop the RG procedure at an energy scale of the same order of magnitude as the temperature T: clusters (or degrees of freedom) that are already frozen at this energy scale will not be active at this temperature and behave like classical spins (at this temperature). The thermodynamical properties, observables like susceptibility or specific heat, will be determined by the active, i.e. not yet frozen clusters.

It is instructive to have a look at the number and size of frozen clusters as a function of the upper cutoff energy, which we identify now with the temperature T. As one can see from the left panel of figure 2 the number of frozen clusters is zero at high temperatures (simply because $\alpha < 1$) and increases rapidly with decreasing temperature before it reaches a maximum and then decreases. The initial increase is due to the formation of many small clusters that behave like classical spins at the corresponding temperature with moments of the order of 10. The subsequent decrease of the number of clusters correlates with an increase in the size of the clusters as can be seen in the right panel of figure 2 and which is due to the coalescence of small clusters into larger ones at the corresponding temperatures.

With this picture in mind we estimate the zero frequency susceptibility $\chi(T)$ as the sum of two contributions $\chi(T) = \chi_{\rm active}(T) + \chi_{\rm frozen}(T)$, one arising from the active, i.e. non-'frozen' spins, $\chi_{\rm active}(T)$, and one from the 'frozen' ones, $\chi_{\rm frozen}(T)$. In doing this, we assume that the interaction between the frozen and the non-frozen clusters is negligible. $\chi_{\rm active}(T)$ is given by (see also equation (A.7))

$$\chi_{\rm active}(T) = \int_0^\infty \frac{{\rm d}\epsilon}{\epsilon} \rho(\epsilon)(1 - \exp(-\beta\epsilon)), \tag{35}$$

J. Stat. Mech. (2008) P04012

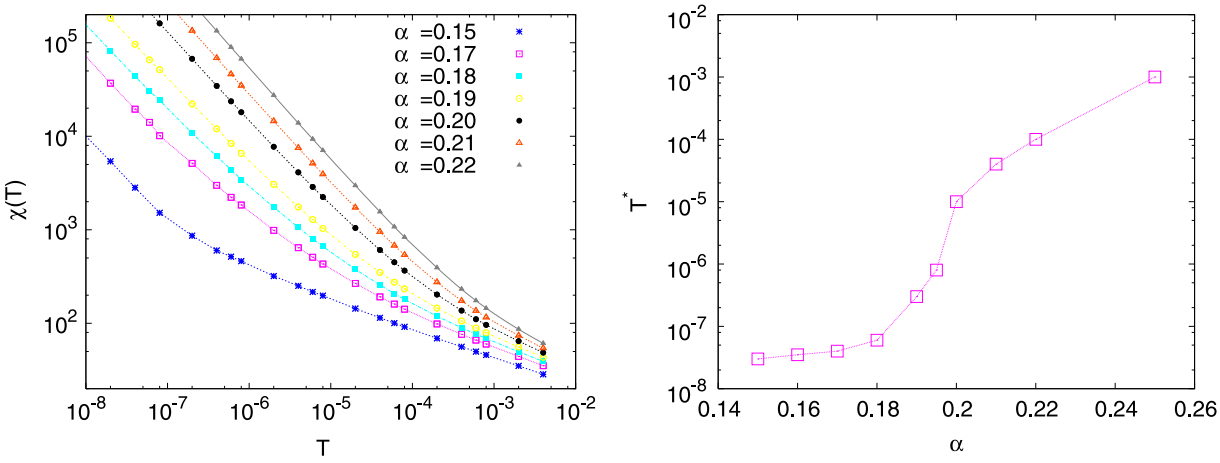

Figure 3. Left: magnetic susceptibility $\chi(T)$ for a disordered chain coupled to an ohmic bath as a function of temperature for different coupling strength α. The susceptibility is calculated as $\chi(T) = \chi_{\rm active}(T) + \chi_{\rm frozen}(T)$ using equations (35) and (36). The size is $L = 4096$, the disorder strength is $h_0 = 1$ and $J_0 = 0.025$. For this value of J_0 the pseudo-critical point is located at $\alpha = 0.2$ [16]. Right: crossover temperature T^* as a function of α extracted from the data on the left panel by the condition $\chi_{\rm active}(T^*) = \chi_{\rm frozen}(T^*)$ (see text).

with $\beta = 1/T$. To estimate the density of states $\rho(\epsilon)$ using our RG scheme we compute the distribution of the amplitudes of fields and bonds which are decimated during the renormalization procedure [1]. Having computed $\rho(\epsilon)$, we then perform numerically the integration in equation (35) to compute $\chi_{\rm active}(T)$. In Griffith's region, where the restricted distribution scales with L as in equation (33), one has $\rho(\epsilon) \propto \epsilon^{-1+1/z}$ and thus $\chi_{\rm active}(T) \propto T^{-1+1/z}$. On the other hand, each (quantum mechanically) frozen spin contributes to the susceptibility by an amount of $1/T$ and thus

$$\chi_{\rm frozen}(T) = \frac{\mathcal{N}_{\rm frozen}(T)}{T}, \tag{36}$$

where $\mathcal{N}_{\rm frozen}(T)$ denotes the number of frozen spins at temperature T and its finite T dependence is computed as explained above. We have computed $\chi(T)$ using our RG scheme for a system of size $L = 4096$ for different values of $\alpha = 0.15, 0.17, 0.19, 0.20$ and 0.22 for $J_0 = 0.025$. In each case, $\chi(T)$ is averaged over 10^4 different realizations of the random couplings and the plots are shown in the left panel of figure 3. Let us first consider the curves for $\alpha < 0.2$, where the restricted distribution $\tilde{P}_L(\log(\Gamma_0/h))$ shows a scaling with L as in equation (33) [16]. For low temperatures still above some temperature T^*, $T > T^*$, one sees in the left panel of figure 3 that $\chi(T)$ is dominated by $\chi_{\rm active}(T) \propto T^{-1+1/z}$, for $\alpha < 0.2$. In this regime of dissipation, one observes that the slope of $\chi(T)$ in a log–log plot depends on α: this is the characteristic of Griffith's behavior. At lower temperature $T < T^*$, $\chi(T)$ is dominated by the $1/T$ behavior of $\chi_{\rm frozen}(T)$ coming from the frozen clusters. Thus figure 3 shows that Griffith's behavior can indeed be observed above T^*. For $\alpha > 0.2$, the susceptibility behaves like $\chi(T) \sim 1/T$ in the whole range of temperature.

In addition, given that we compute separately $\chi_{\rm active}(T)$ in equation (35) and $\chi_{\rm frozen}(T)$ in equation (36) our numerical RG procedure allows us to estimate T^* for

J. Stat. Mech. (2008) P04012

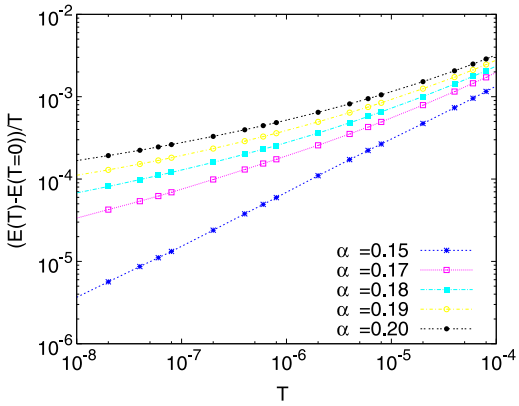

Figure 4. The scaled energy $T^{-1}(\mathcal{E}(T) - \mathcal{E}(T = 0))$, which is proportional to the specific heat $C_v(T)$, for the disordered chain coupled to an ohmic bath as a function of temperature T in a log–log plot. Computations are done using equation (38). The different curves correspond to different values of α. Note that the low temperature behavior is characterized by different slopes for different α, corresponding to a varying exponent $1/z$. The system size is $L = 4096$, the disorder strength $h_0 = 1$ and $J_0 = 0.025$. For this value of J_0 the pseudo-critical point is located at $\alpha = 0.2$ [16].

which these two contributions are equal, $\chi_{\text{active}}(T^*) = \chi_{\text{frozen}}(T^*)$. In the right panel of figure 3, we show a plot of T^* as a function of α. One observes in particular that T^* shows an inflection point as the pseudo-critical point is crossed such that T^* is actually quite small in Griffith's region.

We now turn to the specific heat $C_v(T)$ of the spin degrees of freedom. Assuming that one can also neglect the interaction between frozen and non-frozen clusters one immediately obtains that $C_v(T) = C_{v,\text{active}}(T)$, given that $C_{v,\text{frozen}}(T) = 0$. $C_v(T)$ is thus

$$C_v = \frac{\partial \mathcal{E}(T)}{\partial T}, \tag{37}$$

$$\mathcal{E}(T) - \mathcal{E}(T = 0) = \frac{1}{L} \int_0^\infty \mathrm{d}\epsilon\, \rho(\epsilon)\, \epsilon \frac{\exp(-\beta\epsilon)}{1 + \exp(-\beta\epsilon)}, \tag{38}$$

where $\mathcal{E}(T)$ is the internal energy at temperature T. In Griffith's region where the restricted gap distribution has a finite L scaling as in equation (33), one expects $\mathcal{E}(T) - \mathcal{E}(T = 0) \propto T^{1+1/z}$. Thus $C_v(T) \propto T^{1/z}$ without any cutoff at some temperature T^*. In analogy to $\chi(T)$ we have computed numerically $\mathcal{E}(T) - \mathcal{E}(T = 0)$ (also averaged over 10^4 disordered samples) for different values of α. In figure 4 we show a plot of $T^{-1}(\mathcal{E}(T) - \mathcal{E}(T = 0)) \propto C_v(T)$ as a function of T for different values of α. One observes clearly that the slope decreases as α is increased, i.e. as the critical point is reached. We tried to extract an estimate of the dynamical exponent z by fitting the curves in figure 4 by $T^{-1}(\mathcal{E}(T) - \mathcal{E}(T = 0)) \propto T^{1/z}$ at low T as well as by fitting the curves in the left panel of figure 3 by $\chi(T) \propto T^{-1+1/z}$ for $T > T^*$. Both estimates for z coincide approximately but, since the data shown are close to the pseudo-critical point (which corresponds here to $\alpha = 0.2$), it is rather hard to extract properly the dynamical exponent given that $1/z$

J. Stat. Mech. (2008) P04012

becomes quite small. Thus one would certainly need smaller temperatures to obtain a reliable estimate of z.

We conclude this paragraph by noting that the data in figures 3 and 4 indicate that Griffith's behavior of thermodynamical quantities is observable also in the presence of dissipation.

3.2. Disordered ladder

Our previous study on [16] was restricted to the one-dimensional case. Here, we implement numerically the real space renormalization defined by equations (23)–(25) and equations (27)–(30) for a disordered ladder coupled to a dissipative bath. When considering a ladder (as well as a two-dimensional square lattice) these decimation rules have to be slightly modified to take into account the topology of the system [19]. First, equation (25) has to be modified. In this case, the two spins 2 and 3 are combined to a cluster but when we compute the interactions between this cluster and the rest of the chain, one has to consider the case in which the two original spins 2 and 3 were actually coupled to the same spin i. Although this does not happen in the initial ladder, such a situation may occur during later stages of the renormalization. In this case we set the ferromagnetic coupling of this spin i with the newly formed cluster to

$$\tilde{J}_{i,\mathrm{cluster}} = \max(J_{i2}, J_{i3}). \tag{39}$$

The sum of the two bond strengths could also be taken, but does not make a significant difference when the probability distribution of the bond strengths is broad.

The decimation rule on equation (30) has also to be modified. This rule says that, when the spin on site 2 is decimated, effective interactions are generated between the neighboring sites of 2. But during renormalization of the ladder there might already be bonds J_{ij} present between neighboring sites i and j of site 2. In this case we replace equation (30) by

$$\tilde{J}_{ij} \simeq \max\left(J_{ij}, \frac{J_{i2}J_{2j}}{h_2}\right). \tag{40}$$

The topology of the system changes drastically under renormalization. One starts with a ladder and the decimations change its structure into a random graph, but this change is straightforward to implement numerically.

In the absence of dissipation a critical point was found for $h_0 = 1.9, J_0 = 1$ [19]. In the following we fix $h_0 = 1.9$ and $J_0 = 0.001$ and we vary α. As was done previously for the disordered chain in [16] we first focus on the restricted distribution of the last fields in the samples that are non-frozen (32). For small α, $\tilde{P}_L(h/\Gamma_0)$ displays Griffith's like behavior as in equation (33). In the left panel of figure 5, one plots $\tilde{P}_L(h/\Gamma_0)$ as a function of $\log(\Gamma_0/hL^z)$ with $z = 1.7$ for different system sizes $L = 64, 128, 256, 512$ for $\alpha = 0.2$. The good data collapse of the curves for different L is in good agreement with Griffith's scaling (33). We observe that the dynamical exponent z increases with increasing α. This is depicted in the left panel of figure 6 where one plots again $\tilde{P}_L(h/\Gamma_0)$ as a function of $\log(\Gamma_0/hL^z)$ for different system sizes L but with $z = 7.5$ for $\alpha = 0.262$. However, despite the fact that the gap distribution displays Griffith's behavior, the magnetization is already finite. This can be seen by computing the magnetic moment of the last remaining cluster

J. Stat. Mech. (2008) P04012

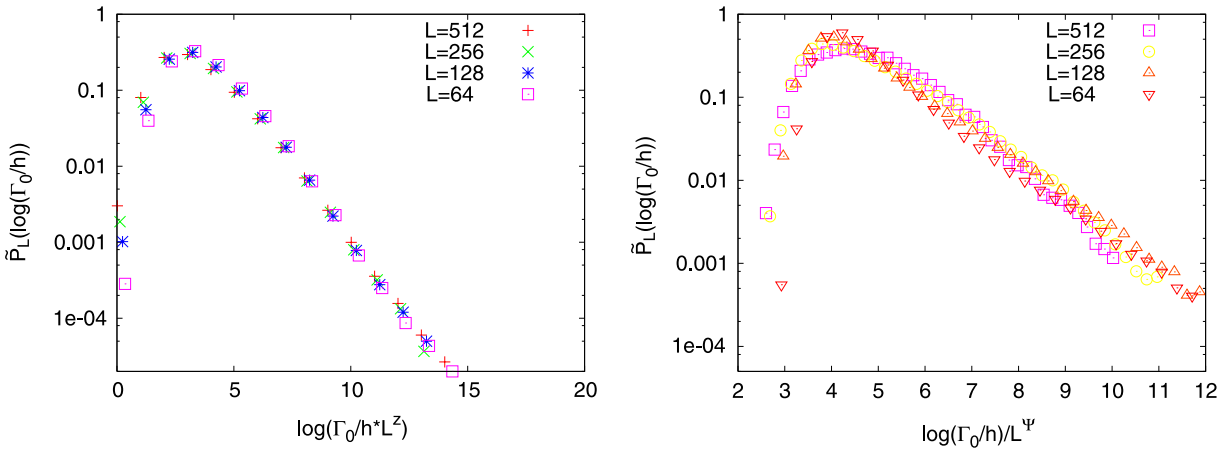

Figure 5. Scaling plot of the restricted distribution $\tilde{P}_L(h/\Gamma_0)$ of the last field to be decimated in the non-frozen samples for the disordered ladder coupled to an ohmic bath. Here $h_0 = 1.9$ and $J_0 = 0.001$. Left: in the Griffiths region ($\alpha = 0.27$): $\tilde{P}_L(h/\Gamma_0)$ as a function of $\log(\Gamma_0/hL^z)$ for different system sizes L. The best data collapse is obtained with the dynamical exponent $z = 1.7$. Right: at the pseudo-critical point ($\alpha = 0.27$): $L^\psi \tilde{P}_L(\Gamma_0/h)$ as a function of $\log(\Gamma_0/h)/L^\psi$ for different system sizes L. The best data collapse is obtained with the exponent $\psi = 0.27(3)$.

as a function of the system size L, see the right panel of figure 6. This behavior, which is due to frozen clusters, is very similar to the one observed for the disordered chain [16].

Finally, one reaches a value of α where z is diverging and one observes a scaling characteristic for an infinite randomness fixed point as in equation (34). This is shown in the right panel of figure 5 where we plot $L^\psi \tilde{P}_L(\Gamma_0/h)$ as a function of $\log(\Gamma_0/h)/L^\psi$ with $\psi = 0.27(3)$.

3.3. Two-dimensional square lattice

We have also implemented the decimation rules in two dimensions for a square lattice. Here also the topology of the system changes drastically during renormalization. In the absence of dissipation a critical point was found for $h_0 = 5.35, J_0 = 1$. Here we include dissipation, fix $J_0 = 0.0001$ and vary α. At small α one observes Griffith's like behavior of the restricted distribution as in equation (33). In the left panel of figure 7, we plot $\tilde{P}_L(\log(\Gamma_0/h))$ as a function of $\log(\Gamma_0/h)$ for different system sizes $L = 8, 16, 32, 64$ and $\alpha = 0.3$. In the right panel, we show that these curves for different L fall on a master curve if one plots them as a function of $\log(\Gamma_0/hL^z)$ with $z = 3.1$. As we increase the value of α, one observes that z is also increasing and eventually we identify a pseudo-critical point, here for $\alpha = 0.37$, where the restricted distribution has a scaling form characteristic for an IRFP as in equation (34) with $\psi = 0.32$. This is shown in figure 8.

4. Super-ohmic dissipation

We have implemented numerically the decimation rules for the super-ohmic bath, which corresponds to $s > 1$. In this case the amplitude $\mathcal{A}$ in equation (18) and $\mathcal{A}'$ in equation (28)

J. Stat. Mech. (2008) P04012

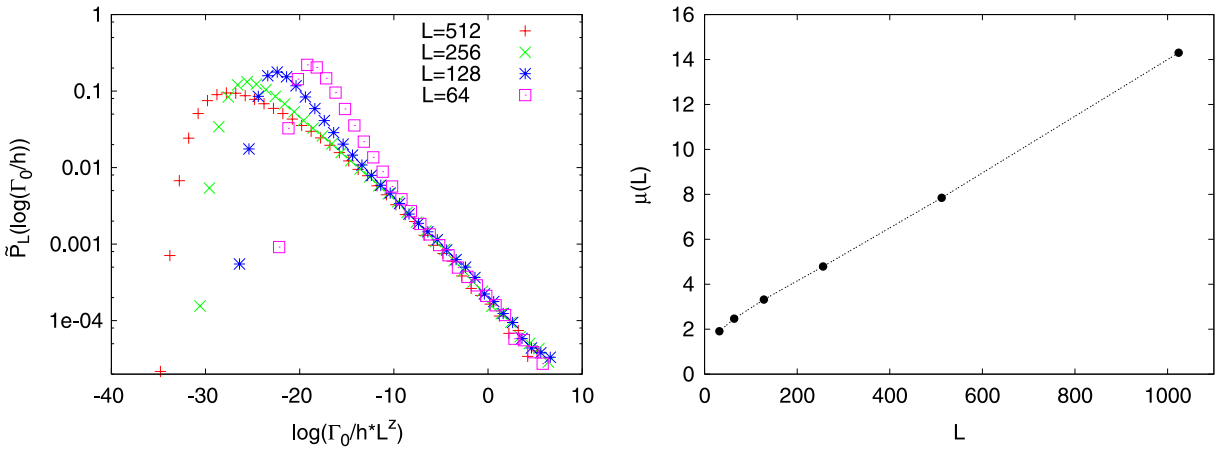

Figure 6. Left: scaling plot of the restricted distribution $\tilde{P}_L(h/\Gamma_0)$ of the last field to be decimated in the non-frozen samples for the disordered ladder coupled to an ohmic bath. Here $h_0 = 1.9$, $J_0 = 0.001$ and $\alpha = 0.262$, i.e. close to the pseudo-critical point at $\alpha = 0.27$. The best data collapse is obtained by the dynamical exponent $z = 7.5$. Right: magnetic moment $\mu(L)$ as a function of L in Griffith's region (parameters as in the left panel). The linear behavior implies a non-vanishing magnetization $m_{\rm eq}$ per spin.

which enter the decimation rules are given by

$$\mathcal{A} = \exp\left(-\frac{\alpha_2}{s-1}\left(1-\left(\frac{pJ_2}{\Omega_2}\right)^{s-1}\right)-\frac{\alpha_3}{s-1}\left(1-\left(\frac{pJ_2}{\Omega_3}\right)^{s-1}\right)\right),$$
$$\mathcal{A}' = \exp\left(-\frac{\alpha_2}{s-1}\left(1-\left(\frac{ph_2}{\Omega_2}\right)^{s-1}\right)\right). \tag{41}$$

For $s > 1$ iterations of the decimation rules (27) always converge to a fixed point value $h_2^* > 0$ given in equation (29). Consequently, the spins cannot be frozen by the dissipative bath.

We first present results for $s = 3$, which corresponds to a phonon bath, and one fixes the coupling to the bath to $\alpha = 0.5$ and the strength of the random transverse field to $h_0 = 1.0$. All data presented here were obtained by averaging over 10^4 different realizations of the disordered couplings.

We first focus on a low value of J_0. In figure 9, one shows a plot of $P_L(\Gamma_0/h)$, the distribution of the transverse field acting on the last remaining cluster, as a function of $\log(\Gamma_0/hL^z)$ for different system sizes with $z = 2.87$. The good data collapse of these different curves suggests that $P_L(h/\Gamma_0)$ exhibits Griffith's behavior:

$$P_L(\log(\Gamma_0/h)) = \mathcal{P}(\log(\Gamma_0/hL^z)). \tag{42}$$

Notice that, at variance with the case of ohmic dissipation (32), one has here $A_L = 1$. If one increases J_0, z is also increasing and for some critical value of $J_0 = J_{0c}$, here $J_{0c} = 0.78$ one observes a scaling characteristic for an IRFP

$$P_L(\log(\Gamma_0/h)) = L^{-\psi}\mathcal{P}_{\rm IRFP}(L^{-\psi}\log(\Gamma_0/h)), \tag{43}$$

J. Stat. Mech. (2008) P04012

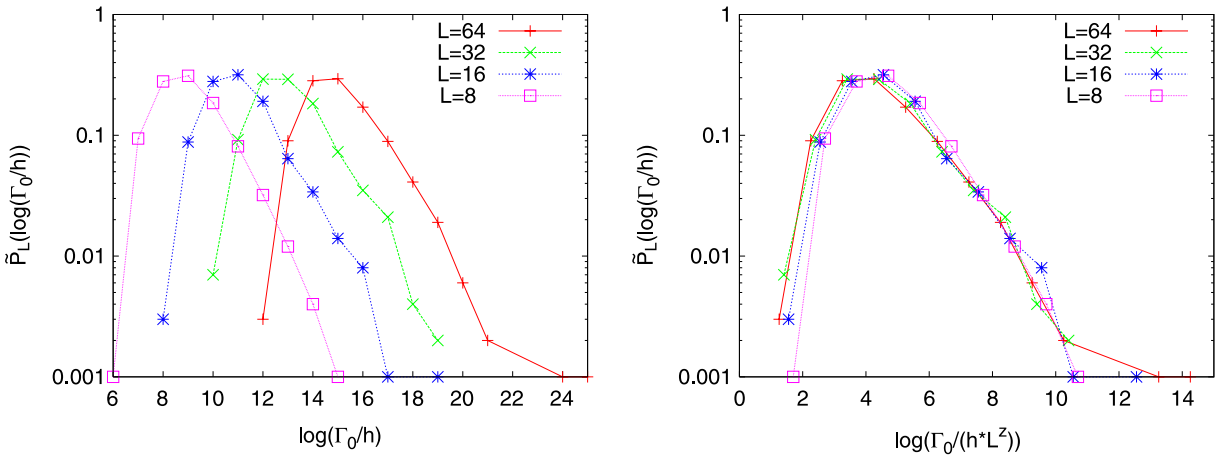

Figure 7. The restricted distribution $\tilde{P}_L(h/\Gamma_0)$ of the last field to be decimated in the non-frozen samples for the disordered square lattice coupled to an ohmic bath. Parameter values fall into the Griffiths region: the disorder strength is $h_0 = 5.35$, $J_0 = 0.0001$ and the coupling to the bath is $\alpha = 0.3$. Left: $\tilde{P}_L(\log(\Gamma_0/h))$ as a function of $\log(\Gamma_0/h)$ for different system sizes L. Right: scaling plot of the data in the left panel: $\tilde{P}_L(\log(\Gamma_0/h))$ as a function of $\log(\Gamma_0/hL^z)$ for different system size L. The best data collapse is obtained with $z = 3.1$.

with $\psi = 1/2$ as in the case without dissipation [3]. This is shown in the left panel of figure 10. In the absence of dissipation random fields and random bonds play a symmetric role in the RTFIC. This is, in principle, not the case when one includes dissipation in the Hamiltonian (1). However, this symmetry is restored asymptotically, close to the critical point. To show this, we have computed $P_L(J/\Gamma_0)$ where J is the last decimated bond. In figure 10 we show a plot of $L^{\psi}P_L(\log(\Gamma_0/J))$ as a function of $(L^{-\psi}\log(\Gamma_0/h))$ with $\psi = 1/2$ for $J_0 = J_{0c}$. The good data collapse, together with the similarities between the plots shown in both panels of figure 10, suggest indeed that this symmetry between bonds and fields is restored at the critical point.

To characterize this IRFP, we have also computed the combinations of the products of the exponents $\varphi\psi$ where φ is another independent exponent associated with this IRFP. This can be measured by computing the disorder averaged correlation function $C(r)$ at the transition. We compute it by keeping track of the clusters during the decimation procedure and compute $C(r) = L^{-1}\sum_i w_{i,i+r}$ where $w_{i,j} = 1$ if the sites i and j belong to the same cluster, and $w_{i,j} = 0$ otherwise. We have checked that, for RTFIC without dissipation at the critical point, this gives the correct exponent [3] within 5% accuracy. A plot of $C(r)$ is shown in figure 11 for different system sizes $L = 64, 128, 256, 512$ and 1024. This plot shows that $C(r) \propto r^{-\eta}$ with $\eta = 0.38(1)$, as in the case without dissipation [3].

We have repeated the same procedure for different values of s and found the critical value $J_{0c}(s)$. We thus obtain the phase diagram in the plane $(J_0, 1/s)$ shown in figure 12 where a critical line separates a paramagnetic phase from a ferromagnetic one. Along this line, we have found a scaling like in equation (43) with an exponent $\psi = 1/2$, independently of s. One can actually estimate the shape of the critical line in figure 12 by assuming that the main effect of dissipation is to reduce the amplitude of the random transverse

J. Stat. Mech. (2008) P04012

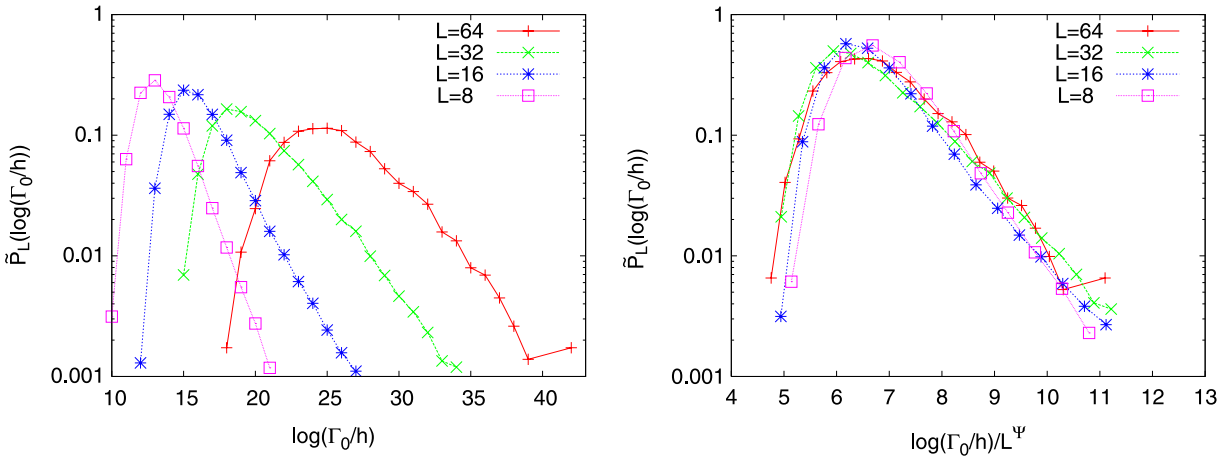

Figure 8. The restricted distribution $\tilde{P}_L(h/\Gamma_0)$ of the last field to be decimated in the non-frozen samples for the disordered square lattice coupled to an ohmic bath. Parameter values correspond to the pseudo-critical point: the disorder strength is $h_0 = 5.35$ and $J_0 = 0.0001$ and the coupling to the bath is $\alpha = 0.37$. Left: $\tilde{P}_L(\log(\Gamma_0/h))$ as a function of $\log(\Gamma_0/h)$ for different system size L. Right: scaling plot of the data in the left panel: $\tilde{L}^{\psi} P_L(\log(\Gamma_0/h))$ as a function of $\log(\Gamma_0/h)/L^{\psi}$. The best data collapse is obtained with the exponent $\psi = 0.32$.

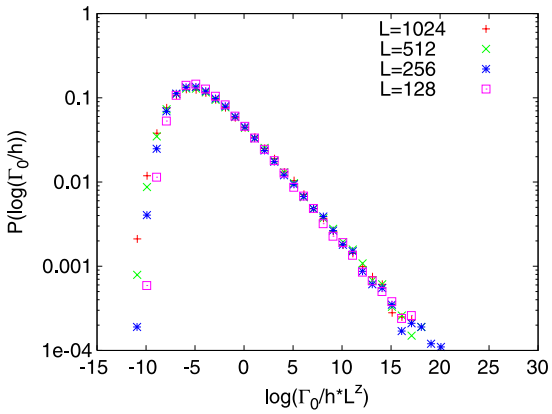

Figure 9. Scaling plot of the probability distribution of the last decimated field for the disordered chain with super-ohmic dissipation, here $s = 3$: $P_L(\Gamma_0/h)$ versus $\log(\Gamma_0/hL^z)$ (scaling in the Griffiths region) for different system size L. The best data collapse is obtained with $z = 2.87$. The disorder strength is $h_0 = 1.0$ and $J_0 = 0.55$ and the coupling to the bath is $\alpha = 0.5$.

field h_0 to h_0^* given by equation (29). If one further assumes that bonds and fields play a symmetric role at the critical point (which is fully compatible with our numerical results in figure 10), the critical point is then given by the relation $J_0 = h_0^*$, as in the RTFIC [3]. This leads to

$$J_{0c} = h_0 \exp\left(\frac{-\alpha}{s-1}\right), \tag{44}$$

J. Stat. Mech. (2008) P04012

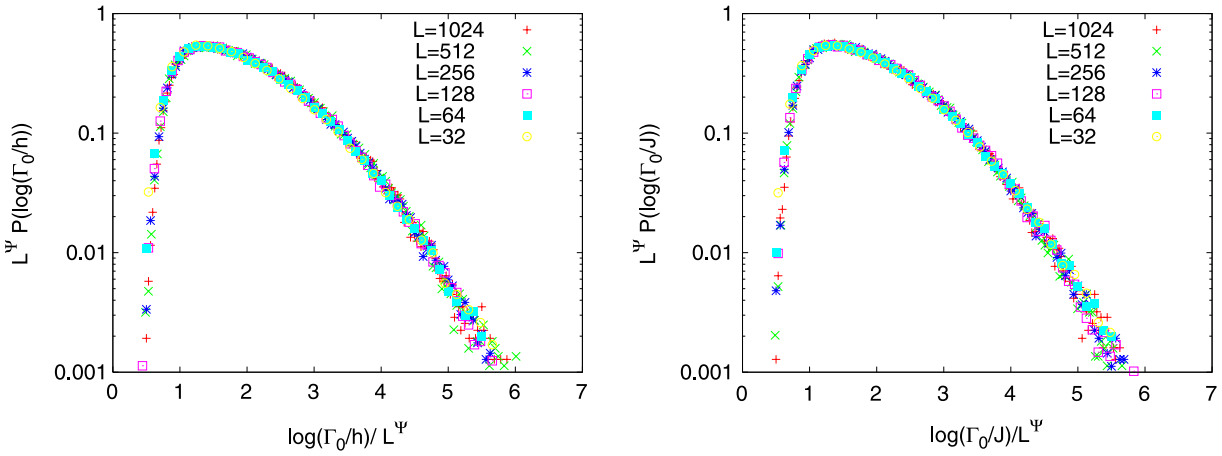

Figure 10. Left: scaling plot of the probability distribution of the last decimated field for the disordered chain with super-ohmic dissipation, here $s = 3$: $L^{\psi} P_L(\log(\Gamma_0/h))$ versus $(\log(\Gamma_0/h))/L^{\psi}$ (IFRP scaling) for different system size L with $\psi = 1/2$. The disorder strength is $h_0 = 1.0$ and $J_0 = 0.55$ and the coupling to the bath is $\alpha = 0.78$. Right: the same as in the left panel but for the bond distribution instead of the field distribution. Note the similarity of the two distributions.

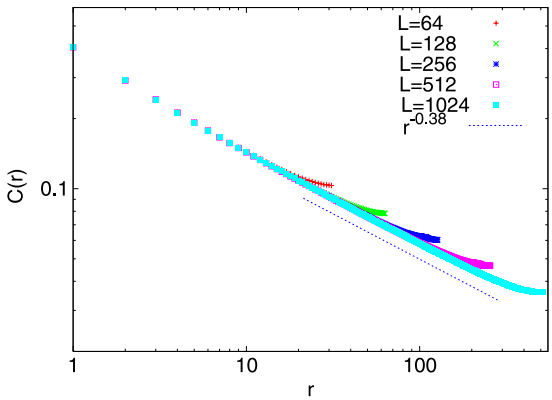

Figure 11. The disorder averaged correlation function $C(r)$ at the critical point for the chain coupled to a super-ohmic bath (here $s = 3$) for different system size L. The disorder strength is $h_0 = 1$ and $J_0 = 0.78$ and the coupling to the bath is $\alpha = 0.5$. The error bars are smaller than the size of the symbols. The decay exponent $\simeq 0.38$ gives $\phi\psi \simeq 0.81$ as in the case without dissipation [3].

which is actually in very good agreement with our numerical estimates for the critical line in figure 12. Using the same arguments, one can also derive analytically the behavior of the dynamical exponent when approaching the critical point. This yields

$$z \propto \frac{1}{2\delta}, \qquad \delta = \frac{1}{2} \log \left(\frac{h_0 \mathrm{e}^{-\alpha/(s-1)}}{J_0} \right), \tag{45}$$

which we have checked to be in good agreement with numerical results.

J. Stat. Mech. (2008) P04012

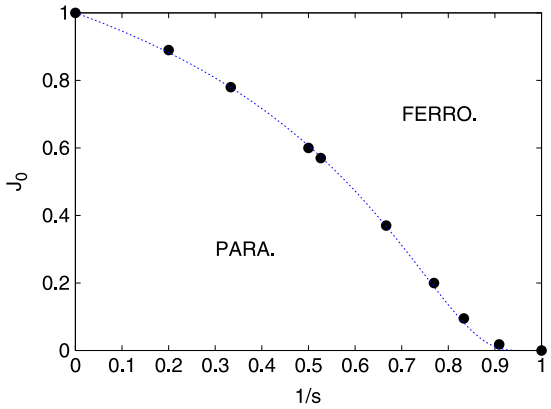

Figure 12. Phase diagram for a disordered chain coupled to a super-ohmic bath (except for $s = 1$) and $h_0 = 1, \alpha = 0.5$. The error bars are smaller than the size of the symbols. Along the line the critical behavior is governed by an IRFP with $\psi = 1/2$ (see figure 10 above). The dashed line is the exact expression of the critical coupling given in the text (44).

Our results thus suggest that, for $s > 1$, the large scale $L > L_s$ properties of the system with super-ohmic dissipation behave at criticality as the dissipationless system. On the other hand, one expects that L_s is diverging when $s \to 1$. To estimate its behavior close to $s = 1$ one observes that the typical energy scale at criticality is given by $E_s \propto h_0 \exp(-\alpha/(s-1))$ (44). But, given that the critical behavior is governed by an IRFP, one expects that $L_s \propto (\log E_s)^{1/\psi}$, with $\psi = 1/2$, see figure 10. Therefore we estimate

$$L_s \propto \frac{\alpha^2}{(s-1)^2}, \tag{46}$$

the length above which the system with super-ohmic dissipation behaves like the one without dissipation.

5. Conclusion

In this paper we have developed a real space renormalization, which combines the SDRG for strongly disordered quantum magnets with the adiabatic renormalization for spin-boson systems, to study disordered, ferromagnetically interacting transverse Ising systems coupled to a dissipative bath. In the important case of ohmic dissipation, we have first extended our previous study in [16] to describe thermodynamical properties. In particular, we have shown that Griffiths–McCoy singularities are visible in the spin specific heat at all temperatures and in the magnetic susceptibility above a (small) temperature T^*. For weak dissipation this temperature is extremely small and system sizes above which classical behavior in the susceptibility becomes visible are extremely large, which represents a major obstacle for numerical studies [21].

We have also shown that the disordered ladder as well as the $2d$ disordered square lattice coupled to a ohmic bath displays the same behavior. Using this real space renormalization, we also studied the case of super-ohmic dissipation ($s > 1$). There

J. Stat. Mech. (2008) P04012

we have found a quantum phase transition described by an IRFP, which is the same as the one found without dissipation. Such a scenario is expected to hold also in higher dimensions.

It would be natural to extend this approach to sub-ohmic dissipation ($s < 1$). Unfortunately, it is well known that in that case the adiabatic renormalization fails to describe correctly the single spin-boson, which in itself has been the subject of recent works [22]. Therefore the problem of an infinite chain (possibly disordered) coupled to a sub-ohmic bath remains a challenging problem which surely deserves further investigations.

A final remark concerns the effect of dissipation upon magnetic systems with a continuous symmetry instead of the discrete (Ising) case we studied in this work. Griffiths–McCoy singularities are much weaker in systems with a continuous symmetry [23], and one would therefore expect that coupling to a dissipative bath would *not* freeze the strongly coupled regions, but enhance their singular behavior. What actually happens can elegantly be classified according to whether rare regions including their long-range interactions in imaginary time due to dissipation are below, at or above their upper critical dimension [15]. A disordered itinerant antiferromagnet, for instance, was recently studied with the strong disorder renormalization group and an infinite randomness fixed point was found [24], including the accompanying algebraic Griffiths–McCoy singularities. On the other hand, non-itinerant antiferromagnets, involving localized magnetic moments, in spatial dimensions larger than 2 like the Heisenberg antiferromagnet on the square lattice, will not show pronounced Griffiths–McCoy behavior since here the Néel ordered ground state is very robust against disorder [25] and no quantum critical point occurs. The effect of dissipation upon strongly disordered magnets thus depends crucially on the effect of disorder itself on the system's ground state.

Acknowledgments

We thank Y C Lin for useful discussions and acknowledge financial support of the Deutsche Forschungsgemeinschaft (DFG). HR thanks the Aspen Center for Physics, where parts of this work were done, for its kind hospitality.

Appendix. A toy model for an Ising chain with ohmic dissipation

To understand qualitatively the full problem described by the Hamiltonian (3) with ohmic dissipation, it is instructive to consider a simpler model where one considers an RTFIC without dissipation but with a finite fraction ρ of zero transverse fields. We thus study in detail in this appendix the RTFIC Hamiltonian with k sites having zero transverse fields ($\rho = k/L$)

$$\mathcal{H} = -\sum_{i=1}^{L} J_i \sigma_i^z \sigma_j^z + \sum_{i=1}^{L} h_i \sigma_i^x \qquad \text{and} \qquad h_{i_1} = \cdots = h_{i_k} = 0. \tag{A.1}$$

First, one immediately sees that the distribution $P_L(h/\Gamma_0)$ shows the same behavior as in equation (32) with $A_L \sim \mathrm{e}^{-L/L^*}$ and in the small ρ limit, $L^* \propto \rho^{-1}$. Besides, the local zero frequency susceptibility is

$$\chi_i(\omega = 0) = \int_0^\beta \mathrm{d}\tau \langle \sigma_i^z(\tau)\sigma_i^z(0)\rangle \tag{A.2}$$

J. Stat. Mech. (2008) P04012

$$= \int_0^\beta \mathrm{d}\tau \frac{1}{\mathcal{Z}} \mathrm{Tr}\{\rho \mathrm{e}^{\mathcal{H}\tau}\sigma_i^z \mathrm{e}^{-\mathcal{H}\tau}\sigma_i^z\}$$
$$= \frac{1}{\mathcal{Z}} \sum_{\{n,m\ (E_n \neq E_m)\}} \frac{\mathrm{e}^{-\beta E_m} - \mathrm{e}^{-\beta E_n}}{E_n - E_m} |\langle n|\sigma_i^z|m\rangle|^2$$
$$+ \frac{1}{\mathcal{Z}} \sum_{\{n,m\ (E_n = E_m)\}} \beta \mathrm{e}^{-\beta E_n} |\langle n|\sigma_i^z|m\rangle|^2, \tag{A.3}$$

where $\{|n\rangle\}$ is a complete basis of eigenvectors of $\mathcal{H}$ (A.1). Their corresponding eigenvalues E_n are such that $E_0 < E_1 < E_2 < \ldots$. The first term in equation (A.3) yields at zero temperature in the non-degenerate case (all transverse fields positive, finite system size L) the known formula

$$\chi_i^{T=0}(\omega = 0) = 2 \sum_{n \neq 0} \frac{|\langle n|\sigma_i^z|0\rangle|^2}{E_n - E_0}, \tag{A.4}$$

since then $\langle 0|\sigma_i^z|0\rangle = 0$ and the last term in equation (A.3) vanishes.

If one or more transverse fields vanish the Hamiltonian becomes block-diagonal. We choose z-representation, such that states can be denoted $\psi = |S_1, \ldots, S_L\rangle$, with $S_i = \pm 1$. For convenience we permute the components such that the site $i_1, \ldots, i_k$ with the k vanishing transverse fields $h_{i_1}, \ldots, h_{i_k}$ stand to the left: $\psi = |S_{i_1}, \ldots, S_{i_k}, S_{j_1}, \ldots, S_{j_{L-k}}\rangle$. All 2^k blocks are identical up to the diagonal part $-\sum_i J_i S_i S_{i+1}$. As a result the two blocks belonging to the states with $S_{i_1} = \cdots = S_{i_k}$ (ferromagnetically aligned 'frozen' spins) have the lowest ground state energy. Obviously

$$\langle \psi|\sigma_{i_p}^z|\psi\rangle = S_{i_p} \qquad \text{for } p = 1, \ldots, k, \tag{A.5}$$

$$\langle \psi|\sigma_i^z|\psi'\rangle = 0 \qquad \text{for } i = 1, \ldots, L, \quad \text{and} \quad (S_{i_1}, \ldots, S_{i_k}) \neq (S'_{i_1}, \ldots, S'_{i_k}). \tag{A.6}$$

At low temperatures ($T \to 0$) the main contributions in the sums in (A.3) comes from the terms with $E_n = E_0$ or $E_m = E_0$, the ground state energy. When $k \neq 0$ there are two ground states $|0_S\rangle$, one with $S = +1$, one with $S = -1$. For $T \to 0 \mathcal{Z}$ can be replaced by $2\mathrm{e}^{-\beta E_0}$, since $\mathcal{Z} = 2\mathrm{e}^{-\beta E_0}(1 + \sum_m \mathrm{e}^{-\beta(E_m - E_0)})$. The two ground states produce also an extra factor 2 (in addition to the one for the sum over $n \neq m$, where either $|n\rangle$ or $|m\rangle$ can be the ground state):

$$\chi_i(\omega = 0) = \frac{4}{2\mathrm{e}^{-\beta E_0}} \sum_{n \neq 0} \frac{\mathrm{e}^{-\beta E_0} - \mathrm{e}^{-\beta E_n}}{E_n - E_0} |\langle n|\sigma_i^z|0\rangle|^2 + \frac{2}{2\mathrm{e}^{-\beta E_0}} \beta \mathrm{e}^{-\beta E_0} |\langle 0|\sigma_i^z|0\rangle|^2$$
$$= 2 \sum_{n \neq 0} \frac{1 - \mathrm{e}^{-\beta(E_n - E_0)}}{E_n - E_0} |\langle n|\sigma_i^z|0\rangle|^2 + \beta |\langle 0|\sigma_i^z|0\rangle|^2. \tag{A.7}$$

The usual argument leading to $\chi_i(\omega = 0) \propto T^{-1+1/z}$ in the Griffiths–McCoy phase of the RTFIC with $k = 0$ involves neglecting the terms $n > 1$ in the first sum in (A.7). This leads to $\chi_i(\omega = 0) \sim (\Delta E)^{-1}$, where $\Delta E = E_1 - E_0$ is the gap, which follows the distribution $P(\Delta) \sim \Delta^{-1+1/z}$. In the present case this distribution has a cutoff at $\Delta_{\min}$ that is exponentially small in L^*, the average distance between sites with zero transverse fields. Thus one expects the first term of (A.7) to display $T^{-1+1/z}$ behavior down to a temperature $T_{\min} = \Delta_{\min}^{z/(z-1)} \sim \mathrm{e}^{-aL^*}$. The second term is $\beta \cdot m_i^2$, where m_i is the

J. Stat. Mech. (2008) P04012

local magnetization in (one of) the ground states and is non-zero due to (A.5). It decays exponentially with the distance x from the nearest frozen site i_p: $m_i\,\mathrm{e}^{-x/2}$. Thus the average over all sites is approximately

$$[m_i^2]_{\mathrm{av}} \sim \frac{1}{L^*/2}\int_0^{L^*/2} \mathrm{d}x\,\mathrm{e}^{-x} \sim \frac{1}{L^*}. \tag{A.8}$$

Thus a T^{-1} behavior coming from the second term in (A.7) with amplitude of order $1/L^*$ competes with a $T^{-1+1/z}$ behavior with amplitude of order 1 coming from the first term in (A.7). The latter dominates for temperatures above a crossover temperature T_{cross}, which is given by

$$T_{\mathrm{cross}} \sim (L^*)^{-z}, \tag{A.9}$$

which is larger than T_{min} (caused by the finite average length L^* of the segments) but still very small when $L^* \gg 1$ (for instance, for $L^* = 10^3$ and $z = 2$ one has $T_{\mathrm{cross}} \sim 10^{-6}$).

References

[1] Fisher D S, 1999 *Physica* A **263** 222
Motrunich O, Mau S-C, Huse D A and Fisher D S, 2000 *Phys. Rev.* B **61** 1160
[2] Iglói F and Monthus C, 2005 *Phys. Rep.* **412** 277
[3] Fisher D S, 1992 *Phys. Rev. Lett.* **69** 534
Fisher D S, 1995 *Phys. Rev.* B **51** 6411
[4] Rieger H and Young A P, 1996 *Phys. Rev.* B **54** 3328
Guo M, Bhatt R N and Huse D A, 1996 *Phys. Rev.* B **54** 3336
[5] Young A P and Rieger H, 1996 *Phys. Rev.* B **53** 8486
Iglói F and Rieger H, 1998 *Phys. Rev.* B **57** 11404
[6] Iglói F, Juhász R and Rieger H, 1999 *Phys. Rev.* B **59** 11308
Iglói F, Juhász R and Rieger H, 2000 *Phys. Rev.* B **61** 11552
[7] Pich C, Young P A, Rieger H and Kawashima N, 1998 *Phys. Rev. Lett.* **81** 5916
Rieger H and Kawashima N, 1999 *Eur. Phys. J.* B **9** 233
[8] Andrade M C *et al*, 1998 *Phys. Rev. Lett.* **81** 5620
Castro Neto A H, Castilla G and Jones B A, 1998 *Phys. Rev. Lett.* **81** 3531
[9] Stewart G R, 2001 *Rev. Mod. Phys.* **73** 797
[10] Castro Neto A H and Jones B A, 2000 *Phys. Rev.* B **62** 14975
Castro Neto A H and Jones B A, 2005 *Europhys. Lett.* **71** 790
[11] Millis A J, Morr D K and Schmalian J, 2001 *Phys. Rev. Lett.* **87** 167202
Millis A J, Morr D K and Schmalian J, 2002 *Phys. Rev.* B **66** 174433
[12] Legget A *et al*, 1987 *Rev. Mod. Phys.* **59** 1
[13] Berche B, Berche P E, Iglói F and Palágyi G, 1998 *J. Phys. A: Math. Gen.* **31** 5193
[14] Vojta T, 2003 *Phys. Rev. Lett.* **90** 107202
[15] Vojta T, 2006 *J. Phys. A: Math. Gen.* **39** R143
[16] Schehr G and Rieger H, 2006 *Phys. Rev. Lett.* **96** 227201
[17] Ma S K, Dasgupta C and Hu C K, 1979 *Phys. Rev. Lett.* **43** 1434
Dasgupta C and Ma S K, 1980 *Phys. Rev.* B **22** 1305
[18] Bulla R, Lee H J, Tonh N H and Vojta M, 2005 *Phys. Rev.* B **71** 045122
[19] Lin Y C, Kawashima N, Igloi F and Rieger H, 2000 *Prog. Theor. Phys. Suppl.* **138** 479
[20] Werner P, Wölker K, Troyer M and Chakravarty S, 2005 *Phys. Rev. Lett.* **94** 047201
[21] Cugliandolo L F, Lozano G S and Lozza H, 2005 *Phys. Rev.* B **71** 224421
[22] Vojta M, Tong N H and Bulla R, 2005 *Phys. Rev. Lett.* **94** 070604
[23] Read N, Sachdev S and Ye J, 1995 *Phys. Rev.* B **52** 384
[24] Hoyos J A, Kotabage C and Vojta T, 2007 *Phys. Rev. Lett.* **99** 230601
[25] Laflorencie N, Wessel S, Läuchli A and Rieger H, 2006 *Phys. Rev.* B **73** 060403(R)

J. Stat. Mech. (2008) P04012